Available online at www.sciencedirect.com

SciVerse ScienceDirect

Acta Materialia 61 (2013) 1136–1145

Acta MATERIALIA

www.elsevier.com/locate/actamat

Basal-plane stacking fault energy of hexagonal close-packed metals based on the Ising model

Qing-Miao Hu *, Rui Yang

Shenyang National Laboratory for Materials Science, Institute of Metal Research, Chinese Academy of Sciences, 72 Wenhua Road, Shenyang 110016, People's Republic of China

Received 16 July 2012; received in revised form 21 October 2012; accepted 24 October 2012
Available online 1 December 2012

Abstract

Stacking fault energy (SFE) plays an important role in the plastic deformation of metals. As compared to those of face-centered cubic metals, the SFEs of hexagonal close-packed (hcp) metals are less reported in literature. In this paper, we derive the expressions of four types (I_1, I_2, E and T_2) of basal plane SFEs of hcp metals in terms of the interlayer interaction energies within the framework of the Ising model. The SFEs of 14 kinds of hcp metals are then evaluated with the interlayer interaction energies extracted from the total energies of four prototypes calculated by using the first-principles full-potential augmented plane-wave method. We show that the hcp metals can be divided into three types according to their interlayer interaction energies. For all the hcp metals involved in this study, I_1 has the lowest SFE, whereas E has the highest. The metals (Mg, Co, Zn and Cd) with principal slip system $(0\,0\,0\,1)[1\,1\,\bar{2}\,0]$ generally have low basal plane SFEs. The I_1 and T_2 SFEs increase linearly with the energy difference between double hexagonal close-packed and hcp structures, whereas the I_2 and E SFEs increase linearly with the energy difference between the short-period twin and hcp structures, indicating a trivial contribution of the interaction energy between atomic layers over third nearest neighbors to the SFEs. The SFEs also correlate with the cohesive energy density (cohesive energy of unit volume) with the exception of Be, Co, Tc and Re.

Keywords: Stacking fault energy; Ising model; hcp metals; First-principles calculations

1. Introduction

Metals deform generally by means of twinning, glide of dislocations or martensitic phase transformation, among which the first two deformation modes are closely related to stacking faults: a deformation twin is generated directly by the formation of a stacking fault and the mobility of the dislocation is highly pertinent to the stacking fault energy (SFE) [1]. For metals with high SFE, a perfect dislocation is unlikely to dissociate into two partials and the metals deform only by dislocation glide. A lower SFE makes the dislocation cross-slip and climb difficult. Due to its importance in the deformation of metals and alloys, stacking faults are a long-standing topic of research in materials science.

The slip plane of face-centered cubic (fcc) metals is mainly the close-packed (1 1 1) plane and the stacking fault is generally induced solely by the "wrong" stacking sequence of the (1 1 1) plane. The SFEs (γ_{SF}) of fcc metals, such as Al, Ni, Cu, Ag, Au, etc., have been extensively investigated both theoretically (e.g. [2–5]) and experimentally (e.g. [6–9]). As to the hexagonal close-packed (hcp) metals, the slip plane can be the basal plane, the pyramidal plane or the prismatic plane depending on the metals [10], alloying elements and deformation temperatures [11]. Therefore, the stacking faults in hcp metals are complicated compared to that in the fcc metals and investigations on the SFE of hcp metals are relatively scarce.

In hcp metals, the basal plane serves as either the principal (e.g. Mg, Zn, Co, Cd) or the secondary slip plane

* Corresponding author. Tel.: +86 024 23971813.
E-mail address: qmhu@imr.ac.cn (Q.-M. Hu).

1359-6454/$36.00
http://dx.doi.org/10.1016/j.actamat.2012.10.023

(e.g. Ti, Zr, Hf) [10]. Therefore, theoretical investigations on the basal plane SFE are highly desirable. The basal plane SFEs of Mg [12–16], Ti [14,17] and Zr [18,19], being important engineering metals, have been studied by using first-principles methods or molecular dynamics (MD) simulations. The SFEs of Mg calculated by Chetty and Winert [13], Smith [14] and Sandlöbes et al. [16] using first-principles pseudopotential methods are in good agreement with each other. However, the SFE of Ti calculated by Smith ($O(10^{-2})$ J m^{-2}), even though close to that from the MD calculations of Zope and Mishin [17], is significantly lower than that evaluated from the experimentally determined stacking fault probability (about 0.31 J m^{-2}) [20]. The basal SFEs of other hcp metals have not been reported in the literature. Since different hcp metals have different slip planes, a systematic investigation on the SFEs of hcp metals is necessary for the understanding of the correlation between the slip character and SFE.

There is actually no reliable experimental technique to measure the SFE. Theoretically, the SFE can be calculated by employing either a supercell or the Ising model. For the supercell model, one constructs a large supercell containing a stacking fault, calculates directly its energy by using first-principles or MD methods, and then evaluates its excess energy over that of the perfect crystal. Within the framework of the Ising model, the SFE is expressed in terms of the interlayer interaction energies, which can be extracted from the total energies of several small size prototypes [21]. The advantage of the Ising model is that the SFE of any type of stacking fault can be evaluated by using the energies of the same series of small sized prototypes and, therefore, is computationally less demanding. Furthermore, a combination of the first-principles methods (e.g. exact muffin-tin orbital method) and coherent potential approximation allows the Ising model to be applied readily to investigate the composition dependence of the SFEs of metals containing alloying elements [22,23], which is very important to the understanding of the alloying effects on the mechanical properties of hcp metals.

In this work, we investigate systematically the four kinds of basal plane SFEs (I_1, I_2, E and T_2) [13] of 14 hcp metals using the Ising model and accurate first-principles calculations. We will show that the basal plane SFE correlates with the slip system of the hcp metals, i.e. metals whose principal slip plane is the basal plane generally have low basal plane SFEs. I_1 and T_2 SFEs (in units of meV) increase linearly with the energy difference between double hcp (dhcp) and hcp structures, whereas the I_2 and E SFEs increase linearly with the energy difference between the short-period twin (spt) and hcp structures. The SFEs (in units of J m^{-2}) also correlate with the cohesive energy density (cohesive energy of unit volume) but with the exceptions of Be, Co, Tc and Re. The carefully and accurately calculated SFEs may serve as benchmarks for experimental measurements and other theoretical calculations.

The rest of the paper is arranged as follows. In Section 2, we derive the SFEs of hcp metals within the framework of the Ising model and then describe the computational method in detail. In Section 3, we present the ground state properties including equilibrium lattice parameters, cohesive energies and bulk moduli of the hcp metals, and then the interlayer interaction energy as well as the SFE. The validity of the Ising model is also verified by comparing the SFEs of Ti and Re from both the Ising and supercell model calculations. The relationship between the calculated SFE and the ground state properties of the metals is discussed later in this section. Finally, we conclude our work in Section 4.

2. Methodology

2.1. Stacking fault energy within the Ising model

Within the Ising model, the energy of the crystals is expressed as:

$$E = J_0 - \sum_k J_k \sum_i S_i S_{i+k}, \tag{1}$$

where J_k is the interaction energy between two atomic layers ($k = 1$ for the nearest neighbors, $k = 2$ for the next-nearest neighbors, etc.). J_0 is energy of the system when all the interlayer interactions are disregarded. S_i is the Ising spin of the ith layer. Taking the fcc sequence with repeating ABC units as the "correct" reference sequence, the spin of the ith layer is $S_i = 1$ if the $(i+1)$th layer follows the "correct" stacking sequence; otherwise, $S_i = -1$. For instance, an A layer with index i has $S_i = 1$ if its next layer $i+1$ is B and $S_i = -1$ if its next layer $i+1$ is C.

With the above definition, Denteneer and Haerigen [21] provided the energies (normalized to the number of layers) of some systems with different repeating units. For the perfect fcc structure with repeating ABC units, the energy is expressed as:

$$E_{\mathrm{fcc}} = J_0 - J_1 - J_2 - J_3 - J_4 - O(J_4), \tag{2}$$

where $O(J_4)$ represents the interaction energies between layers with distance over the fourth-nearest-neigbors. For the perfect hcp structure with repeating AB units:

$$E_{\mathrm{hcp}} = J_0 + J_1 - J_2 + J_3 - J_4 - O(J_4). \tag{3}$$

For the dhcp structure with repeating $ABAC$ units:

$$E_{\mathrm{dhcp}} = J_0 + J_2 - J_4 + O(J_4). \tag{4}$$

For the spt structure with repeating $ABCACB$ units:

$$E_{\mathrm{spt}} = J_0 - \frac{1}{3}J_1 + \frac{1}{3}J_2 - J_3 + \frac{1}{3}J_4 + O(J_4). \tag{5}$$

The energies of the systems with fcc, hcp, dhcp and spt structures can be readily calculated by using first-principles methods. After neglecting the interlayer interaction over the third-nearest-neighboring distance, according to Eqs. (2)–(5), we get the interlayer interaction energy J_k ($k = 0, 1, 2, 3$) as follows:

Table 1
Theoretical ground state properties (lattice parameters a_0 in unit of Å and c_0/a_0), cohesive energy E_{coh} in eV/atom (bulk modulus B_0 in GPa) of hcp metals, in comparison with experimental values [32].

Group	Metal	Method	a_0	c_0/a_0	E_{coh}	B_0	Group	Metal	Method	a_0	c_0/a_0	E_{coh}	B_0
IIA	Be	LSDA	2.226	1.578	4.23	131.8	VIIB	Tc	LSDA	2.709	1.603	8.79	345.6
		PBE	2.263	1.575	3.73	123.5			PBE	2.751	1.604	6.89	301.3
		Exp.	2.27	1.581	3.33	100.3			Exp.	2.74	1.606	/	297.0
	Mg	LSDA	3.150	1.599	1.79	39.5		Re	LSDA	2.737	1.618	9.61	405.5
		PBE	3.211	1.600	1.52	35.8			PBE	2.774	1.621	7.77	366.6
		Exp.	3.21	1.623	1.53	35.4			Exp.	2.76	1.616	8.10	372.0
IIIB	Sc	LSDA	3.237	1.547	4.92	63.2	VIII	Co(SP)	LSDA	2.434	1.611	6.69	258.8
		PBE	3.324	1.558	4.16	55.0			PBE	2.503	1.616	5.06	207.8
		Exp.	3.31	1.592	3.93	43.5			Exp.	2.51	1.621	4.39	
	Y	LSDA	3.548	1.552	4.96	45.6		Ru	LSDA	2.674	1.586	8.76	352.2
		PBE	3.658	1.552	4.23	41.0			PBE	2.720	1.585	6.72	285.9
		Exp.	3.65	1.570	4.38	36.6			Exp.	2.17	1.579	6.62	320.8
IVB	Ti	LSDA	2.861	1.589	6.47	137.3		Os	LSDA	2.715	1.584	10.24	449.9
		PBE	2.935	1.588	5.29	116.0			PBE	2.753	1.584	8.34	400.7
		Exp.	2.95	1.586	4.86	105.1			Exp.	2.74	1.577	/	418.0
	Zr	LSDA	3.154	1.612	7.47	102.8	IIB	Zn	LSDA	2.562	1.875	1.88	87.7
		PBE	3.236	1.600	6.20	93.8			PBE	2.647	1.905	1.10	63.1
		Exp.	3.23	1.594	6.32	83.3			Exp.	2.66	1.861	1.35	59.8
	Hf	LSDA	3.118	1.590	7.52	120.9		Cd	LSDA	2.908	1.886	1.53	62.2
		PBE	3.204	1.586	6.41	106.7			PBE	3.017	1.932	0.73	38.7
		Exp.	3.19	1.583	6.35	109.0			Exp.	2.98	1.886	1.16	46.7

$$J_0 = \frac{1}{2}E_{\mathrm{dhcp}} + \frac{1}{4}E_{\mathrm{fcc}} + \frac{1}{4}E_{\mathrm{hcp}}; \tag{6}$$

$$J_1 = \frac{1}{2}E_{\mathrm{hcp}} + \frac{1}{2}E_{\mathrm{dhcp}} - \frac{1}{4}E_{\mathrm{fcc}} - \frac{3}{4}E_{\mathrm{spt}}; \tag{7}$$

$$J_2 = \frac{1}{2}E_{\mathrm{dhcp}} - \frac{1}{4}E_{\mathrm{fcc}} - \frac{1}{4}E_{\mathrm{hcp}}; \tag{8}$$

$$J_3 = \frac{3}{4}E_{\mathrm{spt}} - \frac{1}{4}E_{\mathrm{fcc}} - \frac{1}{2}E_{\mathrm{dhcp}}. \tag{9}$$

Therefore, the energy of a system with any arbitrary stacking sequence and also the SFE may be evaluated by using J_k ($k = 0,1,2,3$).

Denteneer and Haerigen gave expressions of the energies of the intrinsic and extrinsic stacking faults and the corresponding SFEs of fcc metals in Ref. [21]. For the stacking faults in systems with repeating AB units, Wright has presented the SFE expressions in Ref. [24] without any details. Here, for the completeness of this paper, we derive the SFEs of hcp metals in detail.

There are four kinds of basal plane stacking faults in hcp metals, namely I_1, I_2, E and T_2 [13]. I_1 has stacking sequence $(AB)^m ABCBC(BC)^n$, of which the energy can be expressed as:

$$E_{I_1} = J_0 + \frac{N-2}{N}J_1 - \frac{N-4}{N}J_2 + \frac{N-6}{N}J_3 - \frac{N-8}{N}J_4 - O(J_4) \tag{10}$$

with N being the number of layers contained in the crystal. The corresponding excess energy over that of the perfect hcp structure (i.e. SFE) is therefore:

$$\begin{aligned}\Delta E_{I_1} &= \lim_{N\to\infty} N(E_{I_1} - E_{\mathrm{hcp}}) \\ &= -2J_1 + 4J_2 - 6J_3 + 8J_4 + O(J_4) \\ &= 4E_{\mathrm{dhcp}} + E_{\mathrm{fcc}} - 2E_{\mathrm{hcp}} - 3E_{\mathrm{spt}}.\end{aligned} \tag{11}$$

Similarly, the SFE of I_2 with stacking sequence $(AB)^m ABCAC(AC)^n$ is

$$\begin{aligned}\Delta E_{I_2} &= -4J_1 + 4J_2 - 4J_3 + 4J_4 + O(J_4) \\ &= 2E_{\mathrm{dhcp}} + E_{\mathrm{fcc}} - 3E_{\mathrm{hcp}}.\end{aligned} \tag{12}$$

The SFE of E with stacking sequence $(AB)^m ABCAB(AB)^n$ is:

$$\begin{aligned}\Delta E_E &= -6J_1 + 4J_2 - 6J_3 + 8J_4 + O(J_4) \\ &= 2E_{\mathrm{fcc}} + 2E_{\mathrm{dhcp}} - 4E_{\mathrm{hcp}};\end{aligned} \tag{13}$$

and the SFE of T_2 with stacking sequence $(AB)^m ABCBA(BA)^n$ is:

$$\begin{aligned}\Delta E_{T_2} &= -4J_1 + 8J_2 - 8J_3 + 8J_4 + O(J_4) \\ &= 6E_{\mathrm{dhcp}} + E_{\mathrm{fcc}} - 4E_{\mathrm{hcp}} - 3E_{\mathrm{twin}}.\end{aligned} \tag{14}$$

If presented in terms of the excess energy per unit basal plane area, the SFE may be expressed as:

$$\gamma_{\mathrm{SF}} = \Delta E_{\mathrm{SF}}/S \tag{15}$$

with SF denoting I_1, I_2, E or T_2 types of stacking fault and $S = \frac{\sqrt{3}}{2}a_0^2$ being the area per atom on the basal plane.

2.2. Computational method

The full-potential augmented plane-wave (FP APW) method with local orbitals (lo) based on density functional theory [25], implemented as WIEN2K [26,27], is employed to calculate the total energies of the prototypes with fcc, hcp, dhcp and spt structures. The FP APW+lo method treats the potential and charge density without any shape approximations inside the muffin-tin spheres and in the interstitial region [28]. The wavefunction is constructed with the APW plus local orbitals for the semicore states [29]. The APW with each radial wavefunction is computed at a fixed linearization energy. The local orbitals are evaluated at the same energy as the APWs and vanish at the muffin-tin boundary. The APW+lo scheme leads to significantly smaller basis sets and therefore reduces the computation time compared to the linearized augmented plane-wave (LAPW) method without losing accuracy.

In our calculations, the core states are treated fully relativistically and the valence states scalar relativistically. We perform spin-polarized (SP) calculations for Co and non-spin-polarized calculations for the other metals. The electronic exchange-correlation potential is described within both the local spin density approximation (LSDA) [30] and the generalized gradient approximation parameterized by Perdew, Burke and Ernzerhof (GGA-PBE) [31]. The plane-wave cut-off energy for all metals is set at about 16 Ry. The Brillouin zone is sampled by using Monkhorst–Pack k-point mesh. Our test calculations demonstrate that $12 \times 12 \times 6$ k-point mesh for the hcp structure and similar k-point density for the fcc, dhcp and spt structures are sufficient to yield converged lattice parameters and SFE except for Zn and Cd. For Zn and Cd, a much denser k-point mesh ($24 \times 24 \times 24$ for hcp and similar k-point density for fcc, dhcp and spt) has to be adopted in order to obtain reasonable lattice parameters and SFE. The volume and the lattice parameter c/a of the hcp structure are optimized. The lattice constant a and interlayer distance $d = c/2$ along the z direction of the fcc, dhcp and spt structures are fixed at the optimized a and d of the hcp structure. Note that although we use the term fcc to represent the structure with the repeating ABC sequence, the corresponding structure is not actually the fcc structure of which d/a has to be ideally $\sqrt{3}/3$.

3. Results and discussion

3.1. Ground-state properties of hcp metals

The theoretical ground-state properties of the hcp metals, including lattice parameters, cohesive energy and bulk modulus, are listed in Table 1 in comparison with those obtained from experiments [32].

For all the metals, the lattice constants a_0 from the GGA-PBE calculations are larger than those from the LSDA calculations. This stems from the well-known over-estimation of the binding between the atoms within LSDA. Due to the same reason, the GGA-PBE cohesive energies E_{coh} and bulk moduli B_0 are smaller than the LSDA ones. The GGA-PBE values are in better agreement with experiments, i.e., GGA-PBE gives a better description of the binding between the atoms in these metals.

Although the LSDA generates smaller a_0 than the GGA-PBE does, the lattice parameters c_0/a_0 from both the LSDA and GGA-PBE calculations are close to each other and agree well with experimental values (with error less than about 1.0%) except for Zn and Cd. The GGA-PBE c_0/a_0 of Zn and Cd are significantly larger than the LSDA ones and the latter are in better agreement with experiments. The large c_0/a_0 discrepancy between GGA-PBE and LSDA for Zn and Cd is ascribed to the strong volume dependence of c/a. As shown in Fig. 1a, the c/a of Zn and Cd increase with the volume. With a volume change of about ±5%, the c/a of Zn and Cd change about ±2%, whereas for the other hcp metals, the variation of volume of about ±10% induces a c/a change of no more than ±0.5%. The sensitive dependence of c/a on the volume

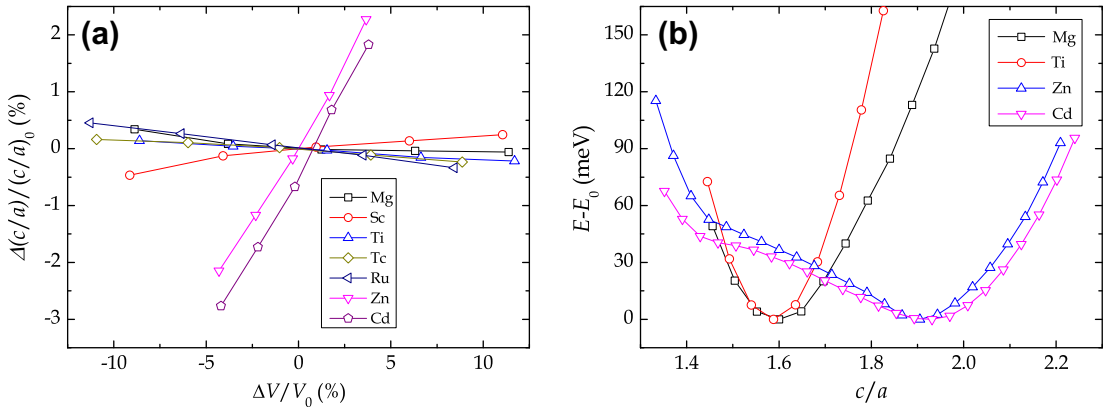

Fig. 1. Lattice parameter c/a vs. volume (a) and energy at equilibrium volume against c/a (b) for some of the hcp metals. The energy presented in (b) is relative to that of the system with equilibrium c/a. The calculations are performed with GGA-PBE.

Table 2
Interaction energies between atomic layers in hcp metals (meV).

Group	Metal	Method	J_1	J_2	J_3	Group	Metal	Method	J_1	J_2	J_3
IIA	Be	LSDA	−41.8	−5.8	−0.6	VIIB	Tc	LSDA	−48.7	−18.8	5.8
		PBE	−44.4	−6.5	−0.6			PBE	−42.5	−17.1	4.7
	Mg	LSDA	−8.6	−1.3	−0.7		Re	LSDA	−36.2	−19.9	2.6
		PBE	−8.2	−1.3	−0.7			PBE	−31.1	−17.5	0.6
IIIB	Sc	LSDA	−23.9	−1.4	−1.7	VIII	Co(SP)	LSDA	−13.6	0.3	0.6
		PBE	−26.5	−1.3	−0.1			PBE	−7.5	−1.4	1.3
	Y	LSDA	−11.1	−4.7	0.8		Ru	LSDA	−59.0	13.1	−9.0
		PBE	−18.0	−1.6	−0.9			PBE	−55.6	12.1	−8.1
IVB	Ti	LSDA	−26.4	10.4	0.3		Os	LSDA	−71.7	15.0	−8.6
		PBE	−30.9	6.4	0.8			PBE	−69.8	13.8	−8.0
	Zr	LSDA	−11.1	14.0	−2.6	IIB	Zn	LSDA	−13.9	−1.6	0.9
		PBE	−18.3	12.6	−2.1			PBE	−11.3	−1.0	1.2
	Hf	LSDA	−31.6	12.1	−2.2		Cd	LSDA	−9.4	−0.5	1.2
		PBE	−37.4	7.3	−0.6			PBE	−6.9	−0.4	3.8

of Zn has also been reported in literature (e.g. [33]). LSDA predicts a smaller volume than the GGA-PBE does. Consequently, the LSDA c_0/a_0 of Zn and Cd are smaller than the GGA-PBE ones.

Besides the unusual c/a vs. V dependence, the energy E vs. c/a at constant volume of Zn and Cd are also different from those of the other hcp metals. As seen in Fig. 1b, the E vs. c/a curves of normal hcp-Mg and hcp-Ti show perfect parabolic behavior. However, the E vs. c/a curves of Zn and Cd deviate significantly from parabolic.

3.2. Interlayer interaction energy and SFE

With the equilibrium lattice constants of the hcp structure determined in Section 3.1, the energies of the systems with fcc, dhcp and spt structure are calculated, and then the interlayer interaction energies J_k are extracted using Eqs. (6)–(9).

In Table 2, we list the interlayer interaction energies J_1, J_2 and J_3. The interaction energies from LSDA and GGA-PBE calculations are quite close to each other. For all the metals, the interaction energy between the nearest-neighboring layers, J_1, is negative, reflecting the attractive interaction in forming the crystal. The absolute values of the interaction energy decrease, in general, from J_1 to J_2 to J_3. In Fig. 2, we plot the ratio of J_2 and J_3 to J_1 for the hcp metals. As seen in Fig. 2, J_3 is only a small fraction of J_1 except for Cd, which rationalizes the truncation of the interlayer interaction at the third-nearest-neighbor distance when calculating the SFE with the Ising model. Cd has quite a large J_3/J_1 since J_1 is already very small. An error of several meV for J_3 may lead to a large change in J_3/J_1. This is possible since the accuracy of the first-principles calculations based on density functional theory is about several meV.

The interaction energy between the second-nearest-neighboring layers, J_2, behaves differently for the metals from different positions of the periodic table. As seen in Fig. 2, J_2/J_1 shows an oscillating behavior for the metals from the left to right side of the periodic table. According to their J_2/J_1 values, the 14 hcp metals can be divided into three types (see Fig. 2). Type I includes the metals from Groups IVB (Ti, Zr, and Hf) and III (Ru and Os) of the periodic table, for which J_2 is positive such that J_2/J_1 is negative. The positive J_2 stabilizes the hcp structure (Eq. (3)) and increases the SFE (Eqs. (11)–(14)). The metals from Groups IIA (Be and Mg), IIIB (Sc and Y) and IIB (Zn and Cd) of the periodic table belong to Type II, for which J_2/J_1 is positive but J_2 is only a small fraction of J_1, indicating that the interlayer interaction is short-ranged. Type III includes the metals from Group VIIB (Tc and Re), for which J_2/J_1 is positive and J_2 is negative with quite a large absolute value (i.e. the interlayer interaction is long-ranged). The large negative J_2 decreases the SFEs significantly and makes the SFE behave very differently from those of other metals. We will come to this point later in Section 3.4.

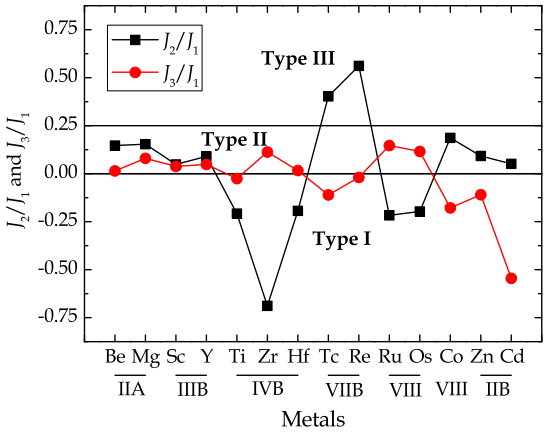

Fig. 2. Ratio of J_2 and J_3 to J_1 of hcp metals from GGA-PBE calculations.

With the interlayer interaction energies listed in Table 2, the basal plane SFEs of hcp metals are calculated according to Eqs. (11)–(15). The SFEs γ_{SF} of the hcp metals are listed in Table 3.

In general, γ_{SF} from the LSDA and GGA-PBE calculations are in good agreement with each other. However, the GGA-PBE γ_{SF} of Co are significantly smaller than those from the LSDA ones and vice versa for Y. The discrepancy may not be ascribed to numerical error since it remains after performing more accurate calculations with denser k-point mesh and higher plane-wave energy cutoff (not shown in this paper). Because GGA-PBE generates better ground state properties of Co and Y than LSDA does, we consider that the GGA-PBE γ_{SF} is more reliable.

As seen in Table 3, the SFEs of different types of stacking fault are different from each other. The magnitude of the SFE determines the stability of the stacking fault. For all the hcp metals, the stacking fault E has the highest SFE, whereas I_1 has the lowest. Therefore, E is the most unstable stacking fault, whereas I_1 is the most stable one.

Among the 14 HCP metals, the basal plane SFEs of Mg, Ti and Zr have been reported in the literature. By using the long-range pair potential computer simulation, Kapinos et al. [18] obtained $\gamma_{I_1} = 0.25\ \mathrm{J\,m^{-2}}$, $\gamma_{I_2} = 0.32\ \mathrm{J\,m^{-2}}$ and $\gamma_E = 0.20\ \mathrm{J\,m^{-2}}$ for hcp-Zr. Although these values agree with the present calculations in order of magnitude, the stability sequence of the stacking faults is different: we predict the stacking fault E to be the most unstable one, whereas Kapinos et al. found E to be more stable than I_1 and I_2. The basal plane SFEs of Mg have been calculated by Chetty and Weinert [13] and Smith [14], both using plane-wave pseudoptential method with a supercell model. Their SFEs (0.02 for I_1, 0.04 for I_2, 0.07 for E, and 0.05 for T_2, all in $\mathrm{J\,m^{-2}}$) are in good agreement with the current calculations. Smith also calculated the SFEs of Ti [14]. Although the reported SFEs (0.00 for I_1, 0.03 for I_2, 0.08 for E, and 0.03 for T_2) are close to the values from the MD calculations with the embedded atom potential performed by Zope and Mishin [17], they are significantly smaller than those calculated in the present work and those evaluated from the experimentally determined stacking fault probability [20].

Different hcp metals have different principal slip planes, a variation that has been ascribed to the c/a ratios of the metals: the hcp metals with c/a ratio larger than the ideal value 1.633 generally have the principal slip plane and direction of $(0001)[1\bar{1}20]$, i.e. the basal plane, whereas those with c/a smaller than 1.633 have the non-basal plane as the principal slip plane [10]. From our calculations, we find that the selection of the principal slip plane also correlates with the basal plane SFE. The absolute value of all four kinds SFEs of Mg, Co, Zn and Cd are quite small (no more than 20 meV for ΔE_{I_1}) from both the LSDA and GGA-PBE calculations. This is also the case for γ_{I_1} and γ_{T_2} of Group VIIB metals Tc and Re. For these metals (Mg, Co, Zn and Cd), the principal slip system is the basal plane slip $(0001)[1\bar{1}20]$ [10]. The metals (e.g., Ti, Zr, Hf) with principal slip systems on the non-basal plane generally have quite high SFEs.

3.3. Comparison between supercell and Ising model calculations

As shown in Section 3.2, the SFEs of Ti calculated in the present work by using the Ising model deviate significantly from those calculated by Smith using a supercell model. Since the atomic relaxation induced by the stacking fault is neglected in the Ising model, one may suspect that the deviation is due to neglecting the atomic relaxation. On the other hand, it is also interesting to know whether or not the slightly negative I_1 and T_2 SFEs of Re and Tc result from neglecting the atomic relaxation. To examine the influence of the atomic relaxation on the SFEs, we also calculated the SFEs of Ti and Re using the supercell model with and without relaxation of the atomic positions as listed in Table 4. It is seen that the effects of atomic relaxation on the SFEs are negligible. The SFEs from the Ising and supercell model calculations are in good agreement with each other, which verifies the validity of the Ising model.

3.4. Correlation of SFE to structure energy difference and ground state properties

Rosengaard and Skriver have shown that the SFEs of the fcc metals vary with atomic number essentially as the energy difference between the fcc and hcp structures [2]. However, they did not present directly the SFE vs. the structure energy difference. Here, we examine the relationship between the basal plane SFEs of hcp metals and the structure energy difference. As shown in Fig. 3, the I_1 and T_2 SFEs (ΔE_{I_1} and ΔE_{T_2} in meV, respectively) increase linearly with the energy difference between the dhcp and hcp structures ($\Delta E^{\mathrm{dhcp\text{-}hcp}}$), whereas the I_2 and E SFEs (ΔE_{I_2} and ΔE_E, respectively) increase with the energy difference between the spt and hcp structures ($\Delta E^{\mathrm{spt\text{-}hcp}}$). The

Table 3
Stacking fault energies γ_{SF} of hcp metals (J m^{-2}).

Group	Metal	Method	I_1	I_2	E	T_2	Group	Metal	Method	I_1	I_2	E	T_2
IIA	Be	LSDA	0.24	0.55	0.86	0.47	VIIB	Tc	LSDA	−0.03	0.24	0.46	−0.00
		PBE	0.24	0.56	0.88	0.47			PBE	−0.03	0.20	0.39	−0.01
	Mg	LSDA	0.03	0.06	0.09	0.06		Re	LSDA	−0.06	0.14	0.30	−0.09
		PBE	0.03	0.06	0.09	0.05			PBE	−0.03	0.14	0.27	−0.05
IIIB	Sc	LSDA	0.09	0.17	0.26	0.17	VIII	Co(SP)	LSDA	0.08	0.17	0.25	0.16
		PBE	0.09	0.18	0.27	0.17			PBE	0.00	0.06	0.09	0.02
	Y	LSDA	0.00	0.03	0.06	0.00		Ru	LSDA	0.58	0.84	1.19	1.07
		PBE	0.05	0.10	0.15	0.09			PBE	0.52	0.76	1.08	0.96
IVB	Ti	LSDA	0.21	0.33	0.45	0.42		Os	LSDA	0.64	0.96	1.36	1.19
		PBE	0.18	0.31	0.44	0.36			PBE	0.59	0.89	1.27	1.11
	Zr	LSDA	0.17	0.21	0.26	0.33	IIB	Zn	LSDA	0.04	0.13	0.20	0.10
		PBE	0.18	0.23	0.31	0.34			PBE	0.03	0.10	0.15	0.07
	Hf	LSDA	0.24	0.35	0.48	0.46		Cd	LSDA	0.02	0.07	0.10	0.05
		PBE	0.19	0.33	0.46	0.38			PBE	−0.02	0.02	0.04	−0.01

slopes for $\Delta E_{I_1} \sim \Delta E^{dhcp-hcp}$, $\Delta E_{T_2} \sim E^{dhcp-hcp}$, $\Delta E_{I_2} \sim \Delta E^{spt-hcp}$, and $\Delta E_E \sim \Delta E^{spt\text{-}hcp}$ lines are 2.38 ± 0.06, 4.38 ± 0.06, 3.38 ± 0.08 and 4.69 ± 0.04, respectively. The relationship between the SFEs and other structure energy differences (e.g. $\Delta E_{I_1} \sim E^{fcc-hcp}$, $\Delta E_{I_1} \sim E^{spt-hcp}$) was also checked in this study, but the linear correlation is not as good as the present ones.

According to Eqs. (2)–(5) and (11)–(14), if the interaction energies over J_3 are neglected:

$$\Delta E_{I_1} = -2J_1 + 4J_2 = 2\Delta E^{dhcp-hcp}, \tag{16}$$

$$\Delta E_{T_2} = -4J_1 + 8J_2 = 4\Delta E^{dhcp-hcp}, \tag{17}$$

$$\Delta E_{I_2} = -4J_1 + 4J_2 = 3\Delta E^{spt-hcp}, \tag{18}$$

and

$$\Delta E_E = -6J_1 + 4J_2 \approx \frac{9}{2}\Delta E^{spt-hcp}. \tag{19}$$

The prefactors on the right side of the above equations are close to the corresponding fitting slopes in Fig. 3a–d. The excellent linear relationships between the SFEs and the structure energy differences suggest that the SFEs of hcp metals may even be evaluated simply by calculating the energies of two prototypes and J_3 plays a trivial role in the SFEs.

From Eqs. (16)–(19), it is obvious that the long-range effect of the interlayer interaction energy J_i as discussed in Section 3.2 affects the stability sequences of different types of stacking faults. For all the metals, I_1 always has the lowest SFE and E has the highest as determined by the smallest (2) and largest (6) prefactors of J_1 for ΔE_{I_1} and ΔE_E, respectively. The prefactors (4) of J_1 are the same for ΔE_{I_2} and ΔE_{T_2}. For those metals (Be, Mg, Sc, Y and Zn) with short-range interlayer interaction energies (very small J_2/J_1), the SFEs are dominated by J_1, and, therefore, ΔE_{I_2} and ΔE_{T_2} are close to each other. For the metals (Ti, Zr and Hf) with negative J_2/J_1 of large absolute values, ΔE_{I_2} is lower than ΔE_{T_2}, whereas for the metals (Tc and Re) with large positive J_2/J_1, ΔE_{I_2} is higher than ΔE_{T_2}. The stability sequences of different types of stacking faults as discussed above are confirmed by our first-principles calculated SFEs as listed in Table 3.

One may also expect that the SFE correlates with the ground state properties of the metals. In general, stronger cohesion between the atoms implies higher overall resistance to the slip deformation, and a larger interlayer distance reduces the interlayer interaction energy. Therefore, the SFE ΔE_{SF} should increase with ΔE_{coh} but decrease with increasing interlayer distance. If presented as γ_{SF}, the SFE should increase with the cohesive energy density E_{coh}/V_0 with V_0 being the equilibrium volume per atom.

Fig. 4a–d presents the SFEs γ_{SF} as a function of E_{coh}/V_0. For all four types of stacking faults, γ_{SF} increases linearly with E_{coh}/V_0 except for Be, Co, Tc and Re. The linear fitting parameters and correlation coefficient

Table 4
The SFEs (J m^{-2}) of hcp-Ti and hcp-Re from supercell calculations in comparison to those from the Ising model. The values in the parentheses are calculated without atomic relaxation.

			Ti		Re	
	Supercell size	Fault number	γ_{SF} (Supercell)	γ_{SF} (Ising)	γ_{SF} (Supercell)	γ_{SF} (Ising)
I_1	ABABABCBCBCB	2	0.17 (0.18)	0.18	−0.03 (−0.02)	−0.03
I_2	ABABABCACACB	2	0.32 (0.32)	0.31	0.09 (0.09)	0.14
E	ABABABCABABAB	1	0.42 (0.42)	0.44	0.21 (0.22)	0.27
T_2	ABABABCBABAB	1	0.35 (0.37)	0.36	−0.10 (−0.09)	−0.05

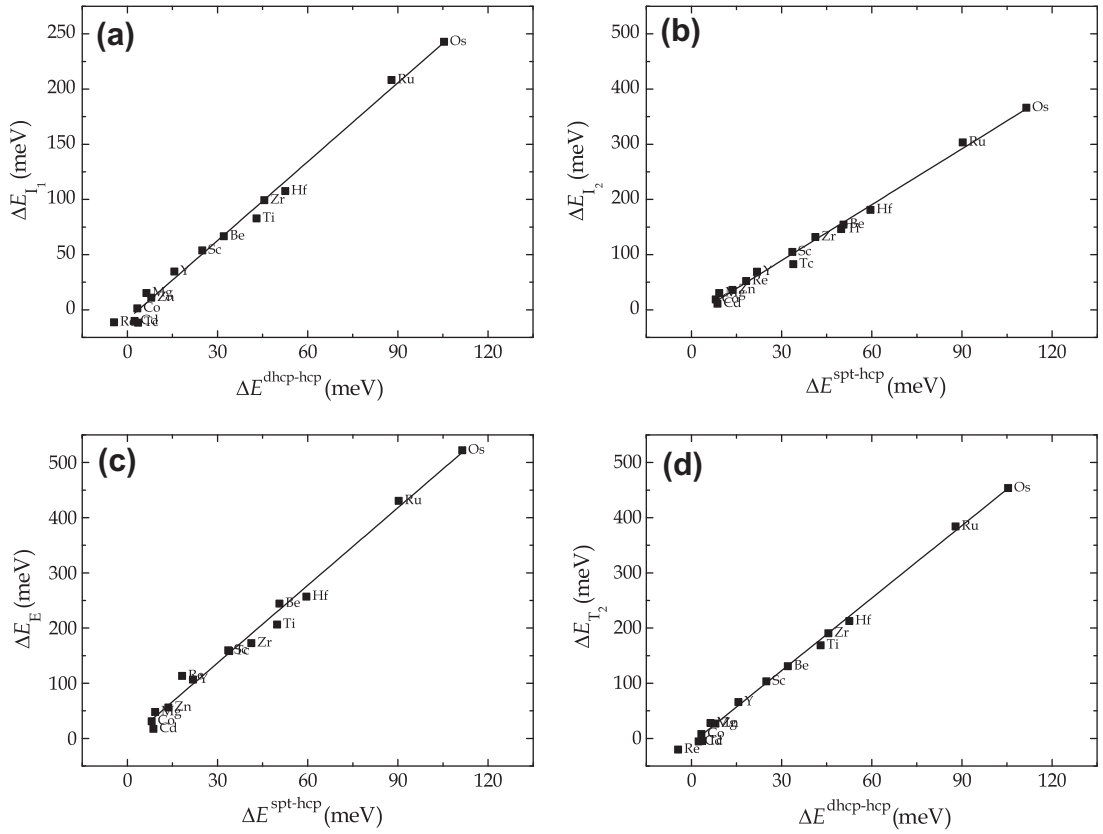

Fig. 3. SFEs ΔE_{SF} (SF = I_1, I_2, E and T_2) as functions of the energy differences in the structures ($\Delta E^{dhcp/twin-hcp}$) from GGA-PBE calculations.

(Pearson's r) are listed in Table 5. The Pearson's r are close to 1, showing the high quality of the linear fit.

As shown in Fig. 4, Be, Co, Tc and Re deviate significantly from the linear correlation. However, their deviations have different origins. For Tc and Re, J_2 is significantly negative and amounts to about 0.4–0.6 times J_1, which reduces greatly the SFE according to Eqs. (11)–(14). For Be, on the one hand, J_2 is negative and thus decreases the SFE. On the other hand, the lattice constant is very small and, therefore, $\Delta E_{coh}/V_0$ is relatively large. For Co, although the cohesive energy is quite high, the interlayer interaction energy J_1 is unusually low, leading to low SFEs. An examination of Tables 1 and 2 shows that a high cohesive energy generally corresponds to a large absolute value of J_1. The calculated PBE cohesive energy of Co (5.06 eV/atom) is at the same level as that of Ti (5.29 eV/atom) whereas J_1 of Co (−7.5 meV) is only 0.24 times of J_1 of Ti (−30.9 meV). We consider that the inconsistency between the interlayer interaction energy and the cohesive energy of Co might be due to the magnetic effect that favors the in-plane but not the interplane binding between the Co atoms.

4. Conclusion

In conclusion, the four types (I_1, I_2, E and T_2) of basal plane SFEs of 14 hcp metals are calculated by using first-principles full-potential augmented plane-wave method and the Ising model. The interlayer interactions between the basal planes have different features depending on the positions of the hcp metals in the periodic table, according to which the hcp metals can be divided into three types. For all the hcp metals involved in this study, I_1 has the lowest SFE, whereas E has the highest. The metals with low basal SFE generally have their principal slip system on the basal plane. The I_1 and T_2 SFEs increase linearly with the energy

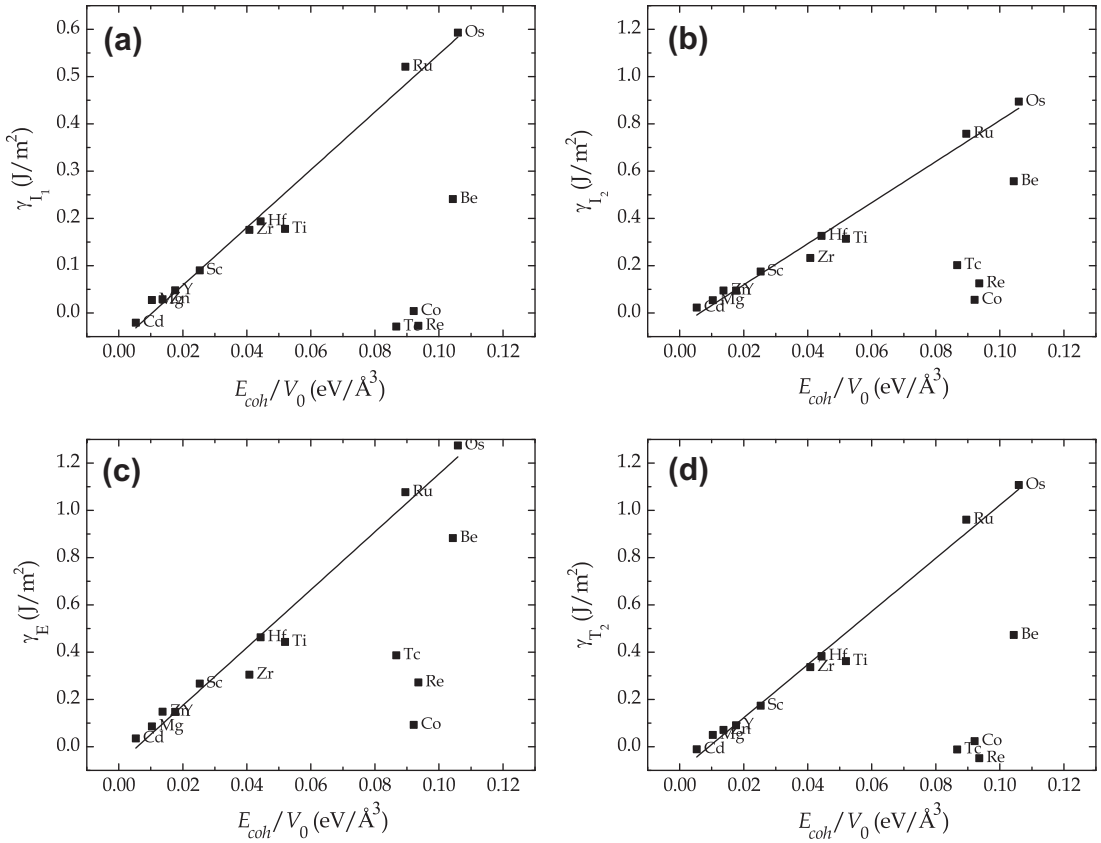

Fig. 4. SFEs γ_{SF} (SF = I_1, I_2, E and T_2) as functions of cohesive energy difference E_{coh}/V_0 from GGA-PBE calculations.

Table 5
Linear fitting parameters and correlation coefficient (Pearson's r) for the SFE γ (J m^{-2}) against the cohesive energy density (E_{coh}/V_0) (eV/Å^3).

	Intercept	Slope	Pearson's r
I_1	-0.064 ± 0.017	6.110 ± 0.319	0.989
I_2	-0.055 ± 0.022	8.692 ± 0.433	0.990
E	-0.070 ± 0.036	12.244 ± 0.702	0.987
T_2	-0.103 ± 0.026	11.250 ± 0.501	0.992

difference between dhcp and hcp structures, whereas the I_2 and E SFEs increase linearly with the energy difference between the spt and hcp structures, indicating a trivial contribution of the interaction energy between atomic layers over third-nearest neighbors to the SFEs. The SFE also correlates linearly to the cohesive energy density for the hcp metals with the exceptions of Be, Co, Tc and Re.

Acknowledgments

The authors are grateful for financial support from NSF of China under grant no. 51271181 and the Chinese MoST under grant Nn. 2011CB606404.

References

[1] Feng Duan et al. Physics of metals I: structure and defects. Beijing: Science Press; 1998.
[2] Rosengaard NM, Skriver HL. Phys Rev B 1993;47:12865.
[3] Nie X, Wang R, Ye Y, Zhou Y, Wang D. Solid State Commun 1995;96:729.
[4] He G, Rong Y, Xu Z. Sci China E 2000;43:146.
[5] Meyer R, Lewis LJ. Phys Rev B 2002;66:052106.
[6] Seeger A, Brener R, Wolf H. Z Phys 1959;155:247.
[7] Susuki H, Barrett CS. Acta Met 1958;6:156.
[8] Thornton PR, Hirch PB. Philos Mag 1958;3:738.
[9] Fullman RL. J Appl Phys 1951;22:448.
[10] Bacon DJ, Vitek V. Metall Meter Trans A 2002;33:721.
[11] Williams JC, Baggerly RG, Paton NE. Metall Meter Trans A 2002;33:837.
[12] Han J, Su XM, Jina ZH, Zhu YT. Scripta Mater 2011;64:693.
[13] Chetty N, Weinert M. Phys Rev B 1997;56:10844.
[14] Smith AE. Mater Forum 2007;31:71.
[15] Datta A, Waghmare UV, Ramamurty U. Acta Mater 2008;56:2531.
[16] Sandlöbes S, Friàk M, Zaefferer S, Dick A, Yi S, Letzig D, et al. Acta Mater 2012;60:3011.
[17] Zope PR, Mishin Y. Phys Rev B 2003;68:024102.
[18] Kapinos VG, Osetsky YN, Platonov PA. J Nucl Mater 1992;195:83.
[19] Udagawa Y, Yamaguchi M, Tsuru T, Abe H, Sekimura N. Philos Mag 2011;91:2665.
[20] Guo Z, Miodownik AP, Saunders N, Schille HP. Scripta Mater 2006;54:2175.
[21] Denteneer PJH, van Haeringen W. J Phys C: Solid State Phys 1987;20:L883.
[22] Vitos L, Korzhavyi PA, Johansson B. Phys Rev B 2006;96:117210.
[23] Lu S, Hu QM, Johansson B, Vitos L. Acta Mater 2011;59:5728.
[24] Wright AF. J Appl Phys 1997;82:5259.
[25] Dreizler RM, Gross EKU. Density functional theory. Berlin: Springer; 1998.
[26] Schwarz K, Blaha P, Madsen GKH. Comput Phys Commun 2002;147:71.

[27] Blaha P, Schwarz K, Madsen GKH, Kvasnicka D, Luitz J. WIEN2k, An augmented plane wave+local orbitals program for calculating crystal properties, Karlheinz Schwarz, Techn. Universität Wien, Austria; 2001.
[28] Wimmer E, Krakauer H, Weinert M, Freeman AJ. Phys Rev B 1981;24:864.
[29] Sjstedt E, Nordström L, Singh DJ. Solid State Commun 2000;114:15.
[30] Kohn W, Sham LJ. Phys Rev A 1965;137:1697.
[31] Perdew JP, Burke K, Ernzerhof M. Phys Rev Lett 1996;77:3865.
[32] Kitte C. Introduction to solid state physics. New York: John Wiley and Sons Inc; 1971.
[33] Steinle-Neumann G, Stixrude L, Cohen RE. Phys Rev B 2001;63:054103.